CHEMISTRY OF MATERIALS

ARTICLE

pubs.acs.org/cm

Mesoporous IrO_2 Films Templated by PEO-PB-PEO Block-Copolymers: Self-Assembly, Crystallization Behavior, and Electrocatalytic Performance

Erik Ortel, Tobias Reier, Peter Strasser, and Ralph Kraehnert*

Department of Chemistry, Technical University of Berlin, Strasse des 17 Juni 124, 10623 Berlin, Germany

ABSTRACT: Synthesis of mesoporous iridium oxide films via soft templating and evaporation-induced self-assembly is demonstrated employing an amphiphilic triblock-copolymer PEO-PB-PEO. Films possess nanocrystalline walls and feature locally ordered pores of about 16 nm diameter. Analysis of the film properties by SEM, TEM, EDX, XPS, SAXS, XRD, and BET along the thermal treatment that succeeds dipcoating shows that the polymer template is removed by calcination between 200 and 300 °C, accompanied by uniaxial shrinkage of film and pore system perpendicular to the substrate. Treating the film in excess of 450 °C leads to further growth of crystallite size and loss of surface area progressing gradually with increasing calcination temperature. Templated IrO_2 films conditioned at 450 °C show substantially reduced electrocatalytic overpotentials (efficiency increases) for the oxygen evolution reaction (OER) compared to those of untemplated coatings. Pore templating thus enables direct control over surface catalytic properties of iridium oxide.

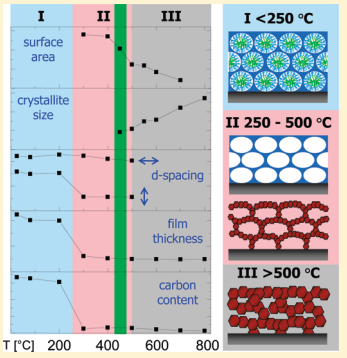

KEYWORDS: mesoporous materials, iridium oxide films, PEO-PB-PEO template, electro catalyst, OER

INTRODUCTION

Materials based on iridium oxide are versatile and attractive candidates for numerous applications, such as supercapacitors,[1] electrochromic materials,[2−4] stimulating neural electrodes,[5−7] and microelectrode for pH sensing.[8−13] Electrodes containing iridium were also used as catalyst for the electro-catalytic chlorine evolution reaction[14] and oxygen evolution reaction ("OER") as anodic part of the electrosplitting of water into hydrogen and oxygen.[15−21] In fact, iridium oxide is commonly selected as an anode material for the OER in strong acidic environment, because it is the only suitable material, in terms of both stability and activity. Its significant cost demands therefore the synthesis of iridium-based catalysts with the highest possible activity, which can be greatly facilitated by nanostructuring of the material as demonstrated in this work.

Films composed of IrO_2 can be synthesized by a variety of methods like sputtering,[1,6,18,22] electrodeposition,[5,12,15,23] spray deposition,[3] or atomic layer deposition.[24] Moreover, chemical methods starting from precursors such as iridium chloride were used in combination with dip- and spin-coating to create iridium oxide coatings on substrates such as ITO-coated glasses and titanium.[2,4,25]

Many applications of oxide films (sensing, catalysis, or electrochemistry) benefit from increased surface area of such coatings, which can be achieved by nanostructuring of the material leading to increased porosity and thus higher surface area and improved accessibility of the surface for reactive species. Iridium oxide coatings with increased surface area yet disordered porosity have been produced in different chemical or electrochemical ways. For example, solutions containing an iridium salt and a rare earth salt were dipcoated onto titanium substrates followed by a heat treatment. The resulting oxide of the rare earth was subsequently removed by exposure to 0.5 M H_2SO_4, leaving a porous Ir oxide layer behind. Such layers possessed mesopores with a wide size distribution ranging from 2 to 10 nm.[25,26] Nakagawa et al. deposited a highly porous film consisting of IrO_x-nanoparticles onto a glassy carbon electrode via controlled-potential electro-flocculation starting from ∼2 nm nanoparticles prepared by thermal hydrolysis of K_2IrCl_6 at pH 13.[16] El Sawy et al. prepared Ir films by electrodepostion of $H_2IrCl_6 \cdot xH_2O$ in 0.5 M H_2SO_4. Films possessed 50% porosity and featured pore sizes between 5 and 25 nm. The deposited Ir films were subsequently converted electrochemically into Ir oxide.[27]

In general, better control over pore size and pore connectivity of oxide coatings can be achieved employing hard or soft templates with narrow size distribution as pore-directing agent. Typically employed porogens are polymer spheres (macro pores) or micelles of amphiphilic block-copolymers (mesopores). Due to an increase in accessible active surface area porous materials show improved performance as electrochemical device[28] as reported, for example, by Jiang et al. for macroporous Ir oxide films featuring pores of about 0.5−0.6 μm diameter derived from polystyrene microsphere templates.[4] In contrast to macroporous materials, the synthesis of templated mesoporous iridum oxide films with narrow and controllable pore size distribution has not been reported so far.

The present study reports the synthesis as well as structural, compositional, and electrocatalytic properties of periodically ordered mesoporous IrO_2 coatings. Pores were templated by micelles of amphiphilic block-copolymers using "evaporation-induced self assembly" (EISA);[29,30] this represents the first successful preparation

Received: March 16, 2011
Revised: May 3, 2011
Published: June 06, 2011

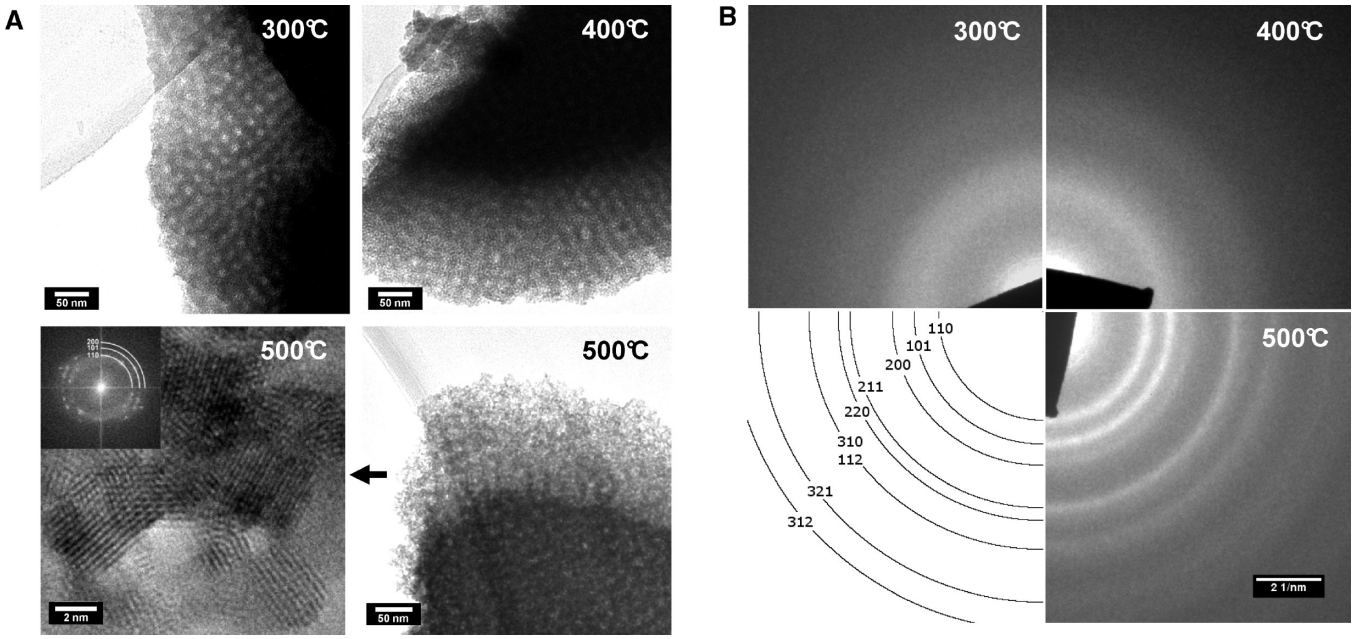

Figure 1. (A) TEM analysis of templated mesoporous IrO_2 film calcined at 300, 400, and 500 °C. The lower left image show a HRTEM analysis of the 500 °C sample with a corresponding FFT plot (inset). (B) SAED patterns corresponding to the TEM images shown in A. The lower left image represent the hkl indices of crystalline IrO_2 (PDF-No.: 150870).

of mesoporous iridium oxide coatings using soft templating. Moreover, special emphasize is placed on understanding the evolution of crystallinity and pore structure of iridium oxide, because catalyst stability in the oxygen evolution reaction crucially depends on forming crystalline walls, whereas pores are essential for obtaining high surface areas and thus optimal catalytic performance.

Employing a wide range of characterization techniques, the present study provides fundamental insights into the formation and crystallization behavior of mesoporous Ir oxide films as well as the templating properties of PEO-PB-PEO polymer templates. The evolution of the oxide coatings structure and porosity is elucidated analyzing materials calcined at different temperatures ranging from 80 to 800 °C. Pore morphology and pore order as well as the crystallinity of the resulting Ir oxide films were investigated by transmission and scanning electron microscopy (TEM, SEM), selected-area electron diffraction (SAED), 2D small-angle X-ray scattering (2D-SAXS), and X-ray diffraction (XRD). Moreover, film composition and film porosity were studied by energy-dispersive X-ray spectroscopy (EDX) and physisorption measurements, respectively, to follow removal of the polymer that served as a pore template. Activity measurements of the mesoporous IrO_2 films for the electrocatalytic splitting of water revealed significantly reduced overpotentials on the porous surfaces, resulting in improved catalytic energy efficiencies.

EXPERIMENTAL SECTION

Film Synthesis. Silicon wafers as well as titanium cylinders were coated with iridium oxide films via dip-coating and subsequent thermal treatment. Prior to coating, Si wafers were cleaned with ethanol, whereas titanium cylinders were polished by SiO_2-polishing paste, then ultrasonicated in water and finally rinsed with ethanol. Dip coating solutions were prepared adding 450 mg of iridium(III) acetate (Heraeus, 48.8% Ir content) and 90 mg of a polymer template poly(ethylene oxide)-b-poly(butadiene)-b-poly(ethylene oxide) (containing 18 700 g/mol PEO and 10 000 g/mol PB, from Polymer Service Merseburg GmbH) to a volume of 3 mL of ethanol. Dip coating was performed in a controlled atmosphere at a temperature of 25 °C and a relative humidity of 40% using a substrates withdrawal rate of 200 mm/min. The as-synthesized films were then immediately heat treated for 5 min inside a preheated muffle furnace in an atmosphere of flowing air. Temperatures for the heat treatment ranged from 80 to 800 °C. For the synthesis of untemplated IrO_2 films a dip-coating solution of identical composition was used, yet without addition of the polymer template. Moreover, the same conditions were applied for dip-coating and calcination as for templated films.

Instrumental Techniques. Transmission electron micrographs (TEM) were recorded on a FEI Tecnai G^2 20 S-TWIN instrument operated at 200 kV on film samples scraped off from the substrates. SEM imaging was performed using a JEOL 7401F instrument at an acceleration voltage 10 kV and at a working distance of 4 mm. To determine the film thickness coated silicon wafers were split in two pieces and imaged in cross section. Image J Version 1.39u (http://rsbweb.nih.gov/ij) was employed to determine the pore diameter, film thickness and to derive FFT plots from the SEM images.

Elemental composition of freshly coated silicon wafers was measured at accelerating voltages of 5 and also at 10 kV by EDX (Bruker Quantax 400) attached to the SEM. EDX analysis on different positions of each film did not show significant differences for the elemental composition of the films, thus indicating homogeneous coatings. XPS spectra were acquired on a KRATOS AXIS 165 spectrometer with Mg Kα X-ray source (225 W). The hydrocarbon C1s signal at 284.6 eV was used as the energy reference to correct for charging.

2D SAXS patterns (small-angle X-ray scattering) were recorded on a Bruker Nanostar (three-pinhole collimation system) using a copper anode as X-ray source (Cu Kα radiation), a 2D detector (2-D HI STAR 1024 × 1024 pixels) with a sample-to-detector distance of 670 mm and employing a sample holder that enabled rotation of the sample between 90° and 10° relative to the incident beam. Respective oxide films were coated on thin silicon wafers (50 μm) and analyzed in transmission mode with a beam incident angle of $\beta = 90°$ and $\beta = 10°$ with respect to the film surface. XRD data was measured on a Bruker D8 Advance

dx.doi.org/10.1021/cm200761f |*Chem. Mater.* 2011, 23, 3201–3209

instrument (Cu Kα radiation). The average crystallite size was calculated applying the Scherrer equation to the (110) peak of IrO_2.

Krypton adsorption isotherms for the porous oxide coatings were measured at 77 K with a Quantachrome Autosorb-1-C. Prior to adsorption, the samples were degassed in vacuum at 200 °C. Specific surface areas were calculated from the Brunauer−Emmett−Teller (BET) method. To facilitate a direct comparison, the derived absolute surface area was then related to the geometrical area (planar dimensions) of the coated substrate.

Electrochemistry. Electro catalytic performance for the oxygen evolution reaction (OER) was tested on films coated on polished titanium cylinders with a diameter of 5 mm. All electrochemical experiments were performed in a three-electrode rotating disk electrode (RDE) cell at room temperature using a BioLogic Science Instruments BiStat potentiostat at 1600 rpm. A platinum mesh (99.9%) was employed as counter electrode, whereas a $Hg/HgSO_4$ electrode (calibrated versus a reversible hydrogen electrode, RHE; 717 mV) served as reference electrode. A 0.1 M $HClO_4$ (Sigma-Aldrich, 99.999%) solution was used as supporting electrolyte.

Prior to the experiments, solutions were deaerated by nitrogen. Then cyclic voltammograms (CV) for the catalytic OER activity of each film sample were measured in a potential window between 1.0 and 1.65 V at a scan rate of 6 mV/s. The uncompensated ohmic solution resistance was measured by impedance spectroscopy to correct for ohmic potential drops at higher current densities. Finally, CVs were recorded in a potential window between 0.4 and 1.4 V at a scan rate of 50 mV/s.

RESULTS AND DISCUSSION

General Film Properties. Morphology and crystallinity of mesoporous iridium oxide films were analyzed by TEM and SAED. Figure 1 shows data recorded on samples coated on Si wafers and calcined in air for 5 min at 300, 400, and 500 °C, respectively. The TEM image of the 300 °C sample (Figure 1A, 300 °C) reveals spherical pores with a diameter of about 16 nm. The pore order can be clearly recognized, with pores penetrating the complete sample. TEM images of Ir oxide films heat treated at 400 and 500 °C show a slight deformation of the pore shapes. The deformation can be attributed to the progressing growth of the Ir oxide nanocrystals that form the mesopore walls. High-resolution TEM (HRTEM) micrographs of the sample calcined at 500 °C (Figure 1A lower left) show distinct lattice fringes, indicating that the pore walls are composed of nanocrystalline iridium oxide. Moreover, the corresponding Fourier transformed image (inset in the HRTEM, Figure 1A lower left) reveals diffraction spots that can be assigned to the (110), (101) and (200) *d*-spacings of IrO_2. Both, the position of diffraction spots as well as the orientation of lattice fringes, indicate that the Ir oxide film is composed of randomly oriented IrO_2 nanocrystals.

Figure 1B shows SAED data for films calcined at 300, 400, and 500 °C as well the reference data for crystalline IrO_2 (PDF-No. 150870, Figure 1B lower left). For the 500 °C calcined sample, the position of the hkl- indices coincides clearly with the lattice parameters of crystalline IrO_2. Moreover, weak diffraction rings can be already observed in SAED for mesostructured Ir oxide films heat-treated at 300 °C (Figure 1B, 300 °C), which indicates beginning crystallization of Ir oxides. The SAED image of the sample calcined at 400 °C shows similar weak diffraction rings. The data are in agreement with the literature, where for sputtered iridium oxide films the amorphous−crystalline transition for IrO_2 has been observed already at temperatures as low as 200 to 300 °C.[31,32]

XPS analysis of the films surface composition further corroborates that iridium is present in the films as IrO_2. Figure 2 shows

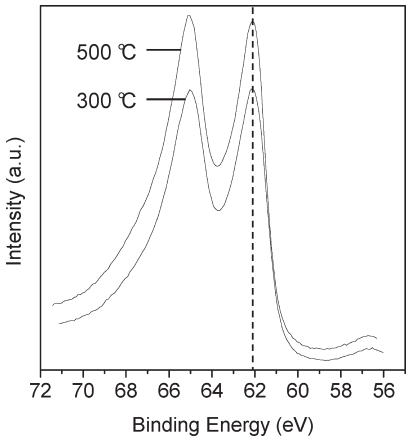

Figure 2. XPS spectra of the Ir4f region of templated mesoporous IrO_2 film calcined at 300 and 500 °C.

XPS spectra of the Ir4f region recorded for mesoporous films that were calcined at 300 °C and at 500 °C, respectively. Both spectra show identical characteristics, with maxima that are positioned at a binding energy of 61.2 eV for the $Ir4f_{7/2}$ peak. The binding energy agrees with the value of 61.2 eV reported in literature for IrO_2,[33] confirming that also the surface of mesoporous films is composed of iridium dioxide.

Evolution of Film Morphology and Chemical Composition upon Thermal Treatment. Films dip-coated on Si wafers at constant withdrawal rate were subsequently calcined at different temperatures between 80 and 800 °C and then analyzed by SEM and EDX to explored film homogeneity, substrate coverage as well as the evolution of film porosity as a function of calcination temperature. Moreover, cross-section SEM images were recorded to follow the temperature-induced film shrinkage.

SEM images corresponding to films calcined at 300, 400, 500, 600, and 700 °C, respectively, are shown in Figure 3 at magnifications of 100 000× (upper row) and 300 000× (lower row). For comparison, images of an untemplated IrO_2 film synthesized in absence of the micelle-forming block-copolymer and calcined at 300 °C are shown in the left column of Figure 3.

The SEM images confirm that in general all films are macroscopically crack free. Moreover, the direct comparison between films synthesized in absence (Figure 3, left column) and presence (Figure 3, all other images) of the template polymer proves that micelles of the PEO-PB-PEO generate mesopores of narrow size distribution which are open to the outer film surface. No pores could be distinguished in SEM images of templated iridium oxide films heat treated at temperatures at 200 °C (not shown), indicating that such low temperatures are insufficient for removal of the polymer template from the coatings.

Templated films calcined at 300 and 400 °C exhibit spherical pore openings of 16 nm in diameter (Figure 3). The mesopores are uniform in size and shape. The FFT-transformed images corresponding to the top-view SEM images (insets in Figure 3, 300 and 400 °C, upper row) show clearly a ring that indicates a well-ordered pore arrangement of differently oriented pore domains, where the periodic distance between pore centers amounted to about 23 nm. The thickness of the pore walls ranges from 5 to 10 nm. SEM images of templated films calcined at 300 and 400 °C recorded at 300 000× magnification (Figure 3, lower row) show that the pore walls exhibit a secondary porosity with pores being smaller than 2 nm in size. This microporosity is also observed in the untemplated IrO_2 film

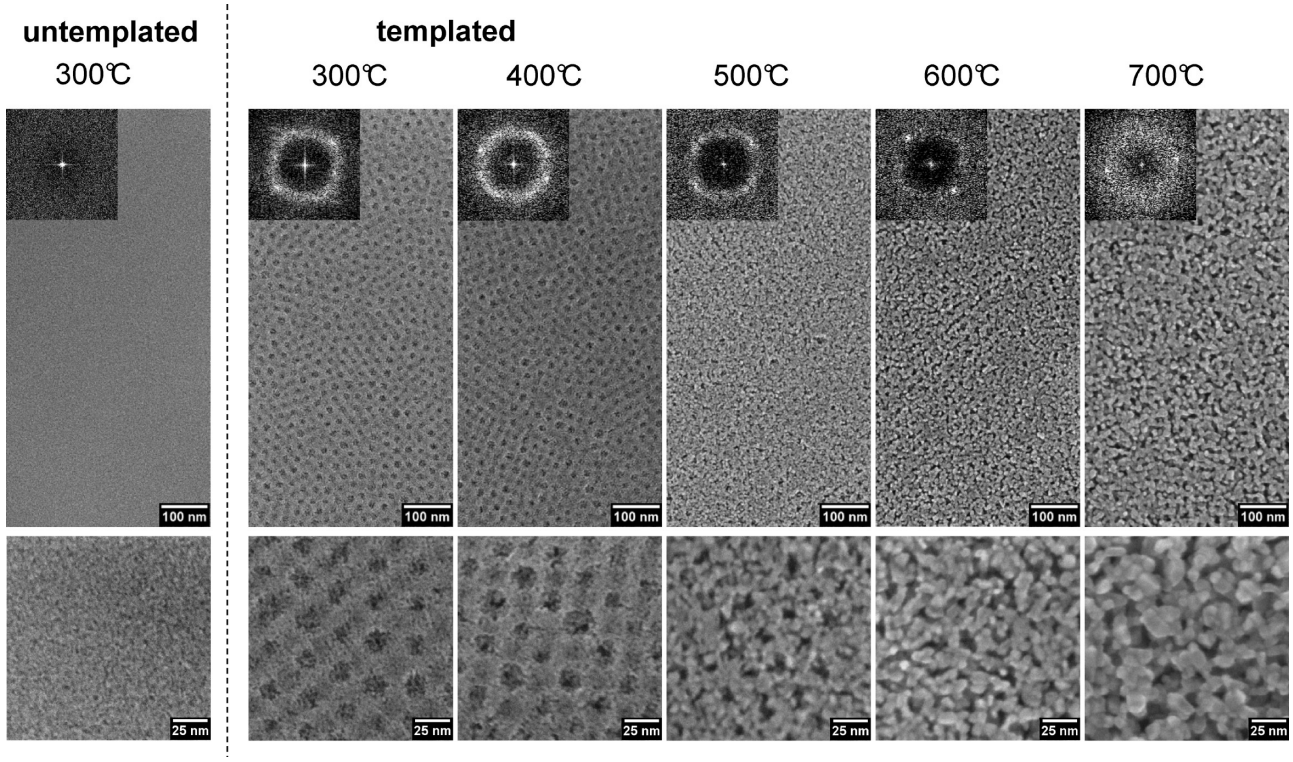

Figure 3. SEM images of mesoporous ("templated") iridium oxide films calcined at 300, 400, 500, 600, and 700 °C (from left to right) imaged at a magnification of 100 000 × (top row) including the respective FFT of the image as inset. Corresponding SEM images at a magnification of 300 000 × are shown in the bottom row. The iridium oxide film prepared without pore template and calcined at 300 °C ("untemplated") is shown for comparison in the left column.

calcined at 300 °C (Figure 3, left column). Hence, the formation of textural microporosity is not related to the presence of the template polymer. One possible explanation for the textural porosity is the generation of CO_2 formed during thermal decomposing of the iridium acetate precursor.

With increasing calcination temperature the shape of templated spherical mesopores starts to degrade (Figure 3, 500 °C). Moreover, films treated at 500 °C show slightly changed pore order, although a distinct ring is still visible in the FFT (Figure 3, 500 °C, inset). Pore walls look more compact and appear to be composed of individual nanoparticles of about 4 to 5 nm in size. Due to crystallization and sintering of Ir oxide, the secondary microporosity in the pore walls, i.e., voids between the individual nanoparticles, becomes more apparent. Films calcined at either 600 or 700 °C show a further increase in the size of the particles that form the pore walls, accompanied by a reorganization of the templated mesoporous structure (Figure 3, 600 and 700 °C) into a so-called "gridlike" structure, which has been observed by Grosso et al. for Pluronic templated TiO_2 films.[34] SEM images of samples calcined at 600 and 700 °C reveal parallel strings of particles, which indicate the preferred gridlike orientation of pores. Moreover, the gridlike mesostructure can be also recognized from the appearance of a pair of bright spots in the FFT's corresponding to the SEM images (inset in Figure 3, 600 and 700 °C). Nevertheless, macroscopic film quality remains excellent, i.e., the further heating does not induce cracking of the films.

The chemical composition of templated iridium oxide films coated onto Si wafers and treated at different calcination temperatures up to 800 °C was analyzed by EDX attached to the SEM at accelerating voltages of 5 and 10 kV. For all films only EDX signals corresponding to carbon, oxygen, iridium and silicon (Si from the substrate) were observed, i.e. the chemical elements that constitute the ingredients of the coating solutions. To reveal the effect of calcination temperature on the removal of polymer template from the film EDX signals were quantified. The derived carbon content (at %) was then related to the iridium content (at %) and normalized in a way that the C: Ir ratio corresponds to 100% for a film before thermal treatment ("25 °C"). Figure 4 illustrates the effect of thermal treatments on various film properties, where in particular Figure 4A details the calculated relative carbon content as a function of calcination temperature. Iridium oxide films heat-treated up to 200 °C show only a small decrease in carbon content of about 8%, whereas a rapid decrease in carbon content of about 84% is detected when the temperature is raised from 200 to 300 °C. Further temperature increases ranging from 300 to 800 °C are not associated with a further significant change in carbon content. The slight initial decrease in carbon content up to 200 °C can be explained by evaporation of residual volatile organic compounds such as ethanol that remained in the film after dip-coating and drying. In contrast, the rapid decrease in carbon observed between 200 and 300 °C is attributed to the removal of the polymer template PEO-PB-PEO from the film by combustion. The fact that the carbon content does not change significantly upon further heating suggests that all carbon stemming from the template polymer is removed from the film between 200 and 300 °C. Such interpretation is in agreement with the fact that templated mesopores were observed by SEM only for films calcined at 300 °C or higher temperatures (Figure 3).

The thickness of coated films was determined from cross-section SEM images as a function of calcination temperature

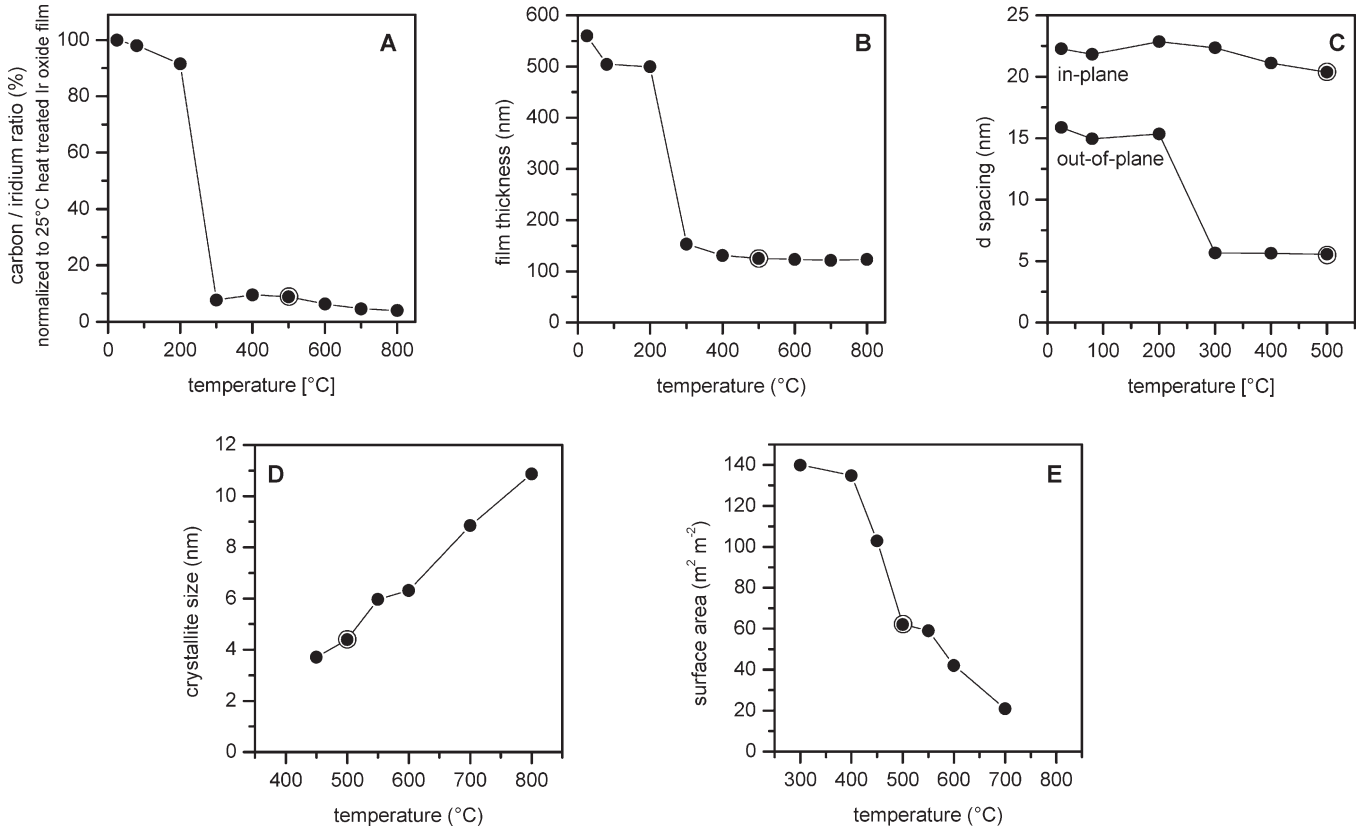

Figure 4. Impact of thermal treatment on properties of templated iridium oxide film: (A) normalized ratio of carbon/iridium derived from EDX analysis (the ratio of carbon content to iridium content (at %) was computed and normalized to the initial value measured before thermal treatment); (B) total film thickness derived from cross-section SEM images; (C) in-plane and out-of-plane *d* spacings derived from 2D-SAXS analysis revealing the film contraction parallel and perpendicular to the substrate; (D) crystallite size from XRD analysis calculated from the FWHM of the (110) IrO_2 reflection using the Scherrer equation; (E) Kr-BET surface area in m^2 of film per m^2 of the substrates planar dimensions. All properties shown as a function of calcination temperature. For better comparison, the values derived for the sample calcined at 500 °C are marked by a circle.

(Figure 4B). The films possess an initial thickness of about 560 nm right after dip-coating ("25 °C"). Heat treatments up to 200 °C induce only minimal film shrinkage. In contrast, extensive film shrinkage from 500 nm to about 150 nm is observed between 200 and 300 °C. A further increase in calcination temperature up to 800 °C does not result in further significant film shrinkage. The observation that a significant decrease in film thickness occurs only between 200 and 300 °C supports the interpretation that removal of the PEO-PB-PEO template from the coated films proceeds in this temperature interval, and proves that the template removal is associated with strong contraction of the film perpendicular to the substrates surface.

In conclusion, dip-coating of substrates in an ethanolic Ir acetate solution employing a PEO-PB-PEO polymer template followed by calcination created homogeneous iridium oxide films with locally ordered mesopore structure. The template stabilizes the mesostructured films up to a temperature of 200 °C, but is completely removed from the films at 300 °C or higher calcination temperatures. Template removal is associated with strong shrinkage of the film perpendicular to the substrate, yet SEM images reveal spherical mesopores openings of 16 nm diameter that are uniform in size and shape.

Pore Ordering. The evolution of the pore order and pore morphology as a function of the heat treatment temperature was analyzed based on 2D SAXS data recorded in transmission mode on films coated on 50 μm thin Si wafers. Figure 5 shows 2D-SAXS patterns of templated films recorded at $\beta = 90°$ (upper row) and $\beta = 10°$ (lower row) between the film surface and the incident beam right after dip-coating ("25 °C") as well as after heat treatments at 200, 300, 400, 500, and 600 °C, respectively.

Right after dip-coating (Figure 5, 25 °C) the SAXS image recorded at $\beta = 90°$ features an isotropic ring, which indicates that the "as-deposited" mesostructured film comprises domains of PEO-PB-PEO micelles that are locally ordered parallel to the substrate. The same sample tilted in a way that the angle between substrate surface and incident beam decreases to β=10° shows also a ring pattern, but with slight deformation toward elliptical shape. Hence, polymer micelles are also ordered perpendicular to the substrate, yet that the cubic pore-solid architecture shows a higher degree of lattice distortions.[35] The *d*-spacing of 22 nm in the *xy*-direction (in-plane, i.e., parallel to the substrate) and 16 nm in the *z*-direction (out-of-plane, i.e., perpendicular to the substrate) obtained from the $\beta = 10°$ scattering image suggests that the drying and solvent evaporation upon film deposition create an elliptically deformed pore morphology typical for sol−gel derived micelle templated films, in which the major axis of the ellipsoid is arranged parallel to substrates surface.[36−38] Hence, the resulting pore morphology differs from an ideal spherical shape due to film shrinkage that occurs preferably perpendicular to the substrate during the EISA process.

SAXS pattern of iridium oxide films calcined at 200, 300 and 400 °C recorded with the substrate positioned perpendicular

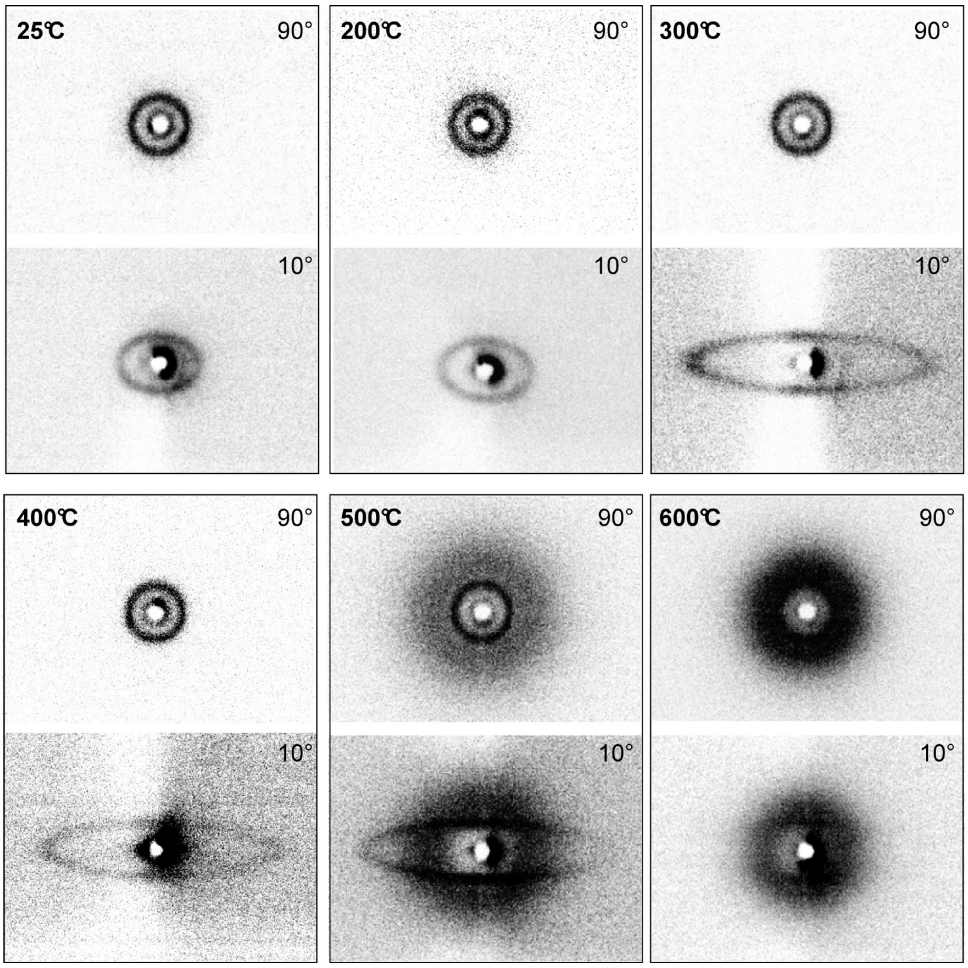

Figure 5. 2D SAXS patterns of templated mesoporous IrO_2 films after thermal treatment at 25, 200, 300, 400, 500, and 600 °C, respectively, recorded in transmission mode with a beam incident angle of $\beta = 90°$ and $\beta = 10°$ with respect to the film surface.

to the beam ($\beta = 90°$) (Figure 5) all display an isotropic ring. The film treated at 200 °C exhibits *d*-spacings of 22 nm (in-plane) and 15 nm (out-of-plane), which is very close to the value observed for the film treated at 25 °C. In contrast, samples treated at 300 and 400 °C film show a strong change in the SAXS patterns, where the shape of the ring becomes elliptically distorted when recorded out of plane, suggesting a contraction of the pore system perpendicular to the substrate. The strong distortion of the pore system observed between 200 and 300 °C coincides with a significant decrease in film thickness (Figure 4B) and removal of carbon (Figure 4A), suggesting that template removal and unidirectional film shrinkage occur concomitant.

SAXS patterns of Ir oxide films treated at 500 °C feature a ring (β=90°) as well as a weak ellipsoid ($\beta = 10°$) with the same *d*-spacings as films treated at 300 and 400 °C, but in addition a diffuse corona appears at higher scattering angles. The diffuse corona is observed at both beam incident angles of $\beta = 90°$ as well as $\beta = 10°$, which indicates these textural feature being independent of the film orientation relative to the substrate. SAXS analysis of materials calcined at 600 °C does not show clear diffraction rings anymore, whereas the corona prevails (Figure 5, 600 °C). The disappearance of the diffraction pattern is attributed to the loss of the cubic mesopore structure, which coincides with the formation of a sintered nanocrystalline surface observed in SEM images (Figure 3, 600 °C).

Appearance of the corona in the 2D SAXS images for samples treated at temperatures exceeding 450 °C could be explained by the formation of increased secondary microporosity, which was observed in SEM for samples treated at 500 °C (Figure 3), where micropores of different size grow in between the ordered mesopores and thus yield a broad additional diffraction signal. Another conceivable explanation is the possibility that the weak ring in the SAXS images originates from X-ray scattering on the individual IrO_2 nanoparticles that are formed upon crystallization at temperatures exceeding 400 °C. Thus, the SAXS pattern could also result from a combination of diffraction (mesopores) and scattering (IrO_2 nanoparticles). The present data does not allow to distinguish between both explanations unambiguously.

To quantify the effect of thermal treatment on the changes of film mesostructure, we depict in Figure 3C the in-plane and out-of-plane *d*-spacings as deduced from the 2D SAXS patterns as a function of calcination temperature. The dimension parallel to the substrate (in-plane) does not show any significant change, i.e., films do not contract parallel to the substrate. In contrast, already after dip-coating and drying (25 °C), the value for the out-of-plane *d* spacing is 30% lower than the in-plane *d* spacing. Moreover, at a temperature of 300 °C, the *d*-spacing in *z* direction decreases drastically from 15 to about 6 nm between. Hence, the template removal at 300 °C is accompanied by a unidirectional contraction of

dx.doi.org/10.1021/cm200761f |*Chem. Mater.* 2011, 23, 3201–3209

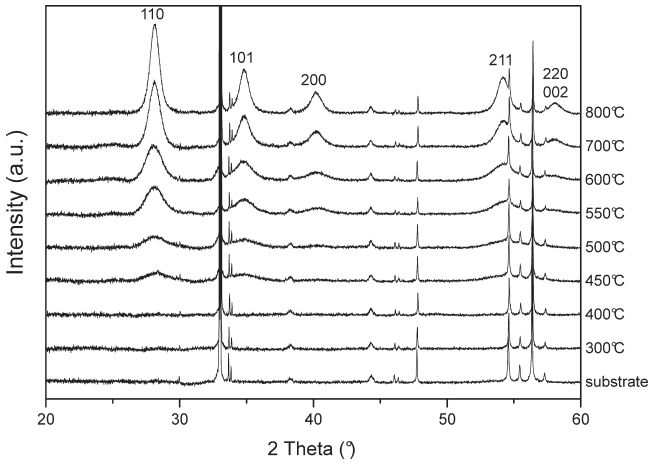

Figure 6. XRD pattern of templated iridium oxide films after calcination at temperatures ranging from 300 to 800 °C, and of the uncoated substrate (Si wafer). Assigned *hkl* indices correspond to crystalline IrO_2 (PDF-No.: 150870).

the pore system perpendicular to the substrate, which does not progress any further above 300 °C.

Crystallinity. In addition to electron diffraction (Figure 1B), crystallization of iridium oxide as well as crystal growth were also followed via X-ray diffraction as a function of calcination temperature. Figure 6 shows diffractograms recorded on films coated onto silicon wafers and then calcined at temperatures ranging from 300 to 800 °C. After heat treatment at 300 and 400 °C only reflections attributable to the substrate (i.e., silicon wafer) can be observed, whereas the more sensitive SAED provided evidence for crystallinity formation already at 300 °C (Figure 1B). Crystalline IrO_2 can be distinguished by XRD starting at temperatures of 450 °C as suggested by the appearance of broad reflections at angles of 28° and 35°. With increasing temperature progressively sharper reflections are observed, suggesting improved crystallinity, and the (110), (101), (200), (211), and (220) reflections of crystalline IrO_2 (PDF-No. 150870) can be clearly distinguished (Figure 6).

To quantify the impact of calcination temperature, we calculated the average crystallite size from the (110) reflection via Scherrer equation. Corresponding values are plotted in Figure 4D. The crystallite size observed at 450 °C amounts to about 4 nm. With increasing calcination temperature the crystallite size continuously increases up to about 11 nm at 800 °C (Figure 4D), suggesting an ongoing sintering process. This observation agrees well with evidence derived from microscopy (Figure 3) that crystallites progressively grow above 400 °C. In conclusion, film texture and crystallinity are controlled by the calcination protocol, and ordered mesoporosity concomitant with crystalline pore walls as desired for application can be achieved in the temperature window of 300−500 °C.

Surface Area. The surface area of nanostructured oxides is an important criterion for many applications. Hence, the surface area of films calcined at different temperatures was analyzed employing Krypton as adsorbate. Figure 4E depicts the evolution of BET surface area normalized to the substrate planar dimensions in m^2 film per m^2 substrate for different calcination temperatures. The BET surface area after thermal treatment of the films at 200 °C and lower temperatures, i.e., before template removal, was too low to be measurable. In contrast, the BET value of 140 m^2 of film per m^2 of substrate measured for a film calcined at 300 °C clearly suggests that at such temperature the polymer template has been removed from the film creating accessible porosity. When increasing calcination temperature to temperatures exceeding 300 °C the surface area continuously decreases, reaching about 20 m^2/m^2 at 700 °C (Figure 4E). This continuous decrease in surface area with increasing calcination temperature is attributed to the sintering of crystallites evidenced by SEM and XRD.

Expressed in units of m^2/g the surface area translates into 248 and 83 m^2/g for samples calcined at 300 and 550 °C, respectively. The values are in agreement with specific surface areas typically observed for other templated inorganic mesoporous oxide films, which were reported in a review by Sanchez et al. to be in the range of 100−250 m^2/g.[39] Moreover, the surface area achieved by pore templating is significantly higher than previous for IrO_2 catalysts reported values, such as the 31 m^2/g deduced by Siracusano for IrO_2 made through the sulfite-complex route and additional calcination at 400 °C.[40] The increased accessible surface area translates directly into improved catalytic performance in the OER reaction as discussed in the next section.

Electrocatalytic Performance. The electrocatalytic performance of mesoporous iridium oxide films for the oxygen evolution reaction (OER) was tested in a three-electrode rotating disk electrode set up. The IrO_2 catalysts were supported on polished titanium cylinders as homogeneous crack-free films. To demonstrate the advantage of ordered mesoporosity, the electro-catalytic behavior of templated mesoporous iridium oxide was compared to that of an untemplated IrO_2 film, both being calcined at 450 °C. Moreover, performance was benchmarked against literature data recently reported by Nakagawa et al. for a film that consisted of 2 nm iridium oxide nanoparticles which was produced by an electro-flocculation method. This benchmark was reported to show a lower overvoltage for OER than previously reported catalysts.[16]

Figure 7 shows the electrochemical response of the prepared films recorded in two different potential windows. The cyclic voltammogram (CV) in the lower electrode potential window of 0.4 - 1.4 V (Figure 7A) provides information on the active surface area of the film.[41−44] Sweeping then to more positive potentials between 1.0 and 1.65 V (Figure 7B, C) the catalytic OER activity of the films was measured.

Figure 7A reveals that the templated IrO_2 film (a) exhibits significantly larger geometric current densities than the untemplated IrO_2 film (b). The current response (normalized to the electrodes geometric surface area) is composed of two different contributions, the double-layer capacitance and a faradaic current according to surface redox couples accompanied by proton inclusion.[45] The current response is about 2.1 times higher on templated IrO_2 films (a) than on untemplated IrO_2 films (b). Both samples show weak faradayic peak characteristics in this potential range, in line with IrO_2 films prepared by Fierro et al. via thermal treatment of iridium metal as well as IrO_2 prepared by thermal decomposition of H_2IrCl_6 solution at 500 °C and samples prepared by Ardizzone at 400 °C.[41,46] The observed differences in the voltammetric charge between templated and untemplated films (Figure 7A) can be attributed to differences in the electrochemically active surface area caused by differences in the coating surface morphology induced by the pore template.[41−44]

The increase in surface area that results from pore templating amounts to a factor of 2.1 when assessed by cyclic voltammetry, whereas physisorption analysis provides a slightly higher factor of 3.0 for films calcined at 450 °C (103 vs 34 m^2/m^2). This difference of about 30% can result either from limited experimental accuracy or the different nature of both techniques. Although physisorption

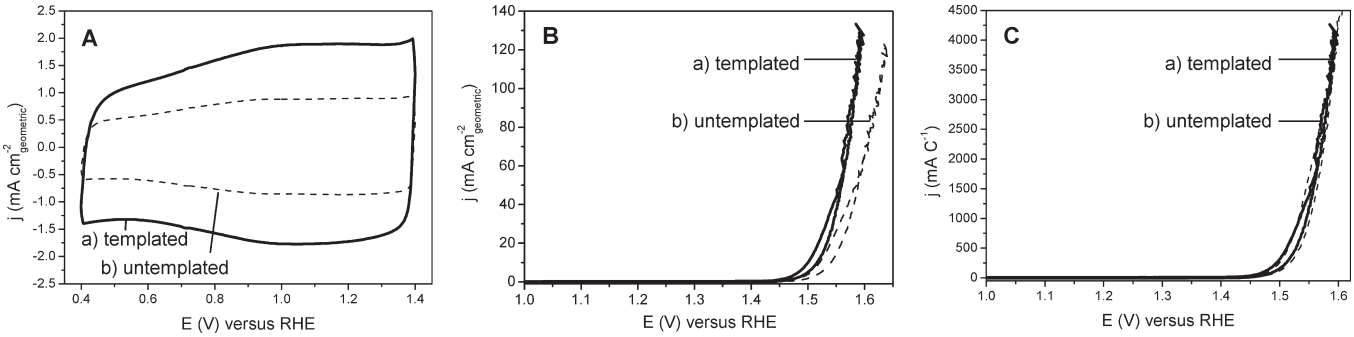

Figure 7. Cyclic voltammograms (CV) for the oxygen evolution reaction recorded on (a) templated (solid line) and (b) untemplated (dashed line) IrO_2 films calcined at 450 °C. (A) CV's in a potential window between 0.4 and 1.4 V recorded with a scan rate of 50 mV/s. (B, C) CV in a potential window between 1.0 and 1.65 V with a scan rate of 6 mV/s. In A and B, the current density *j* is normalized to the geometric (planar) surface area of the working electrode. In C, the current density *j* is normalized to anodic charge derived from scans A. Supporting electrolyte: 0.1 M $HClO_4$.

measures the complete surface that is accessible to small Kr atoms, cyclic voltammetry can assess only the crystallites that are electrically contacted and are accessible to the electrolyte. Hence, the slightly lower value resulting from the electrochemical analysis appears to be reasonable. In the following, the surface area obtained from the CV study is used for normalization of electro-chemical OER rates.

Quasi steady-state voltammetric responses of templated and untemplated IrO_2 based films recorded at a scan rate of 6 mV/s in the oxygen evolution reaction in the higher potential window of 1.0 to 1.65 V were normalized to the electrodes geometric surface area are shown in Figure 7B. Both, templated and untemplated IrO_2 films exhibit significant OER catalytic activity. Moreover, the overpotential of about 0.21 V measured at low geometric current densities of 0.5 mA cm^{-2} is in good agreement with values previously reported for Ir oxide electrodes in literature, i.e. 0.25 V at current density of 0.5 mA cm^{-2}.[16] The thermodynamic minimum potential in the OER under standard conditions amounts to 1.23 V. Curves in Figure 7B, however, clearly indicate that the required overpotential for the templated mesoporous film is substantially lower than that for the untemplated film for all current densities in the OER potential region. Compared at a geometric current density of 100 mA cm^{-2}, the measured overpotential advantage of templated films amounts to more than 40 mV. Assuming for the untemplated film that the BET surface area corresponds approximately to the electrochemically accessible surface area of the iridium oxide and 100% current efficiency, a rate of 3×10^{-10} mol cm^{-2} s^{-1} can be estimated at a potential of 1.5 V.

Finally, Figure 7C shows the catalytic OER voltammetric data in a form that is normalized to the anodic voltammetric charge in the potential window between 0.4 and 1.4 V as depicted in Figure 7A, i.e., the catalytic data are essentially normalized to the active surface area of the coatings and thus represent the intrinsic catalytic activity of the surface. As Figure 7C illustrates, the CVs of the templated and untemplated IrO_2 coatings are almost identical. Thus, the intrinsic catalytic behavior of IrO_2 is identical and not affected by the templating procedure, i.e., the electronic structure of the active centers remains unchanged for templated compared to the untemplated coatings. In consequence, the increased catalytic activity of templated mesoporous IrO_2 film in Figure 7B originates from an increase in accessible surface area resulting from pore templating. Our data evidence that soft-templating of mesopores is very effective to enhance the electrocatalytic performance of iridium oxide, as demonstrated for the case of the oxygen evolution reaction. At constant product yields, i.e., specified amounts of oxygen per electrolysis time, the templated films would afford lower current densities, and accordingly, reduced overpotentials, which would make the process more energy efficient.

CONCLUSIONS

The present study shows for the first time that iridium oxide, one of the most stable OER catalysts, can be synthesized as crystalline IrO_2 films with ordered mesoporosity via evaporation-induced self-assembly (EISA). The synthesis is enabled by a new triblock-copolymer template PEO-PB-PEO. The polymer template is removed from dip-coated films between 200 and 300 °C, creating a film with open mesopores of 16 nm in diameter. Whereas first signs of the desired crystallinity can be detected already at 300 °C, further heating induces growth of the iridium oxide crystals from 4 nm (450 °C) to 11 nm (800 °C), accompanied by a gradual degradation of pore shape as well as a decrease in surface area from 140 (300 °C) to 20 m^2/m^2 (700 °C).

The present study clearly identifies the synthesis pathways and conditions that are essential to achieve a stable and active OER catalyst, which possesses at the same time templated mesopore structure, crystalline pore walls and a large surface area. Respective films conditioned at 450 °C show excellent electrocatalytic performance and stability in the oxygen evolution reaction. Since intrinsic catalytic OER activity remains unaffected by the pore templating, the increased surface area can be fully used to improve overall catalyst performance, permitting thus a significant reduction in the amount of iridium required for an OER catalyst. The demonstrated catalyst optimization shows for the first time how a rational design of crystallinity and porosity of electrocatalysts can be realized synthetically in order to balance active surface area, diffusional access, and catalyst stability. Adapted to other catalysts, pore and crystallinity tuning as demonstrated here will enable significant performance improvements also for other electrochemical processes performed on an industrial scale like the chlorine evolution reaction.

AUTHOR INFORMATION

Corresponding Author

*E-mail: ralph.kraehnert@tu-berlin.de.

ACKNOWLEDGMENT

The authors thank X. Tuaev for recording SAXS data, ZELMI (TU-Berlin) for TEM analysis and K. Halser (Fraunhofer IZM)

for XPS studies. E. Ortel and R. Kraehnert acknowledge generous funding from BMBF within the frame of the Nanofutur program (FKZ 03X5517A). R. Kraehnert, T. Reier and P. Strasser are grateful for the financial support from the German Cluster of Excellence in Catalysis (UNICAT) funded by the German National Science Foundation (DFG) managed by the Technical University Berlin.

REFERENCES

(1) Liu, D. Q.; Yu, S. H.; Son, S. W.; Joo, S. K. *Electrochem. Solid-State Lett.* **2008**, *11* (11), A206–A208.
(2) Nishio, K.; Watanabe, Y.; Tsuchiya, T. *Thin Solid Films* **1999**, *350* (1−2), 96–100.
(3) Patil, P. S.; Mujawar, S. H.; Sadale, S. B.; Deshmukh, H. P.; Inamdar, A. I. *Mater. Chem. Phys.* **2006**, *99* (2−3), 309–313.
(4) Jiang, F.; Zheng, T.; Yang, Y. *J. Non-Cryst. Solids* **2008**, *354* (12−13), 1290–1293.
(5) Mailley, S. C.; Hyland, M.; Mailley, P.; McLaughlin, J. M.; McAdams, E. T. *Mater. Sci. Eng., C* **2002**, *21* (1−2), 167–175.
(6) Lee, I. S.; Park, J. M.; Son, H. J.; Park, J. C.; Lee, G. H.; Lee, Y. H.; Ciu, F. Z. In *Asbm6: Advanced Biomaterials VI*; Zhang, X., Tanaka, J., Yu, Y., Tabata, Y., Eds.; Trans Tech Publications Ltd: Zurich-Uetikon, Switzerland, 2005; Vol. 288−289, pp 307−310.
(7) Lu, Y.; Cai, Z. X.; Cao, Y. L.; Yang, H. X.; Duan, Y. Y. *Electrochem. Commun.* **2008**, *10* (5), 778–782.
(8) O'Hare, D.; Parker, K. H.; Winlove, C. P. *Med. Eng. Phys.* **2006**, *28* (10), 982–988.
(9) Ges, I. A.; Ivanov, B. L.; Werdich, A. A.; Baudenbacher, F. J. *Biosens. Bioelectron.* **2007**, *22* (7), 1303–1310.
(10) El-Giar, E.; Wipf, D. O. *J. Electroanal. Chem.* **2007**, *609* (2), 147–154.
(11) Ges, I. A.; Ivanov, B. L.; Schaffer, D. K.; Lima, E. A.; Werdich, A. A.; Baudenbacher, F. J. *Biosens. Bioelectron.* **2005**, *21* (2), 248–256.
(12) Bezbaruah, A. N.; Zhang, T. C. *Anal. Chem.* **2002**, *74* (22), 5726–5733.
(13) Li, J. P.; Du, Y. L.; Fang, C. *Electroanalysis* **2007**, *19* (5), 608–611.
(14) Mozota, J.; Conway, B. E. *J. Electrochem. Soc.* **1981**, *128* (10), 2142–2149.
(15) Yagi, M.; Tomita, E.; Kuwabara, T. *J. Electroanal. Chem.* **2005**, *579* (1), 83–88.
(16) Nakagawa, T.; Beasley, C. A.; Murray, R. W. *J. Phys. Chem. C* **2009**, *113* (30), 12958–12961.
(17) Marshall, A.; Borresen, B.; Hagen, G.; Sunde, S.; Tsypkin, M.; Tunold, R. *Russ. J. Electrochem.* **2006**, *42* (10), 1134–1140.
(18) Slavcheva, E.; Radev, I.; Bliznakov, S.; Topalov, G.; Andreev, P.; Budevski, E. *Electrochim. Acta* **2007**, *52* (12), 3889–3894.
(19) Dau, H.; Limberg, C.; Reier, T.; Risch, M.; Roggan, S.; Strasser, P. *Chemcatchem* **2010**, *2* (7), 724–761.
(20) Forgie, R.; Bugosh, G.; Neyerlin, K. C.; Liu, Z. C.; Strasser, P. *Electrochem. Solid-State Lett.* **2010**, *13* (4), D36–D39.
(21) Neyerlin, K. C.; Bugosh, G.; Forgie, R.; Liu, Z. C.; Strasser, P. *J. Electrochem. Soc.* **2009**, *156* (3), B363–B369.
(22) Slavcheva, E.; Schnakenberg, U.; Mokwa, W. *Appl. Surf. Sci.* **2006**, *253* (4), 1964–1969.
(23) Petit, M. A.; Plichon, V. *J. Electroanal. Chem.* **1998**, *444* (2), 247–252.
(24) Kim, S. W.; Kwon, S. H.; Kwak, D. K.; Kang, S. W. *J. Appl. Phys.* **2008**, *103* (2), 6.
(25) Yoshinaga, N.; Sugimoto, W.; Takasu, Y. *Electrochim. Acta* **2008**, *54* (2), 566–573.
(26) Murakami, Y.; Nakamura, T.; Zhang, X.-G.; Takasu, Y. *J. Alloys Compd.* **1997**, *259* (1−2), 196–199.
(27) El Sawy, E. N.; Birss, V. I. *J. Mater. Chem.* **2009**, *19* (43), 8244–8252.
(28) Walcarius, A. *Anal. Bioanal. Chem.* **2010**, *396* (1), 261–272.
(29) Brinker, C. J.; Lu, Y. F.; Sellinger, A.; Fan, H. Y. *Adv. Mater.* **1999**, *11* (7), 579–585.
(30) Smarsly, B.; Antonietti, M. *Eur. J. Inorg. Chem.* **2006**, *6*, 1111–1119.
(31) Hackwood, S.; Dayem, A. H.; Beni, G. *Phys. Rev. B* **1982**, *26* (2), 471–478.
(32) Liao, P. C.; Chen, C. S.; Ho, W. S.; Huang, Y. S.; Tiong, K. K. *Thin Solid Films* **1997**, *301* (1−2), 7–11.
(33) Atanasoska, L.; Atanasoski, R.; Trasatti, S. *Vacuum* **1990**, *40* (1−2), 91–94.
(34) Grosso, D.; Soler-Illia, G.; Crepaldi, E. L.; Cagnol, F.; Sinturel, C.; Bourgeois, A.; Brunet-Bruneau, A.; Amenitsch, H.; Albouy, P. A.; Sanchez, C. *Chem. Mater.* **2003**, *15* (24), 4562–4570.
(35) Brezesinski, T.; Smarsly, B.; Iimura, K.; Grosso, D.; Boissiere, C.; Amenitsch, H.; Antonietti, M.; Sanchez, C. *Small* **2005**, *1* (8−9), 889–898.
(36) Grosso, D.; Balkenende, A. R.; Albouy, P. A.; Lavergne, M.; Mazerolles, L.; Babonneau, F. *J. Mater. Chem.* **2000**, *10* (9), 2085–2089.
(37) Brezesinski, T.; Fischer, A.; Iimura, K.; Sanchez, C.; Grosso, D.; Antonietti, M.; Smarsly, B. M. *Adv. Funct. Mater.* **2006**, *16* (11), 1433–1440.
(38) Grosso, D.; Soler-Illia, G.; Babonneau, F.; Sanchez, C.; Albouy, P. A.; Brunet-Bruneau, A.; Balkenende, A. R. *Adv. Mater.* **2001**, *13* (14), 1085–1090.
(39) Sanchez, C.; Boissiere, C.; Grosso, D.; Laberty, C.; Nicole, L. *Chem. Mater.* **2008**, *20* (3), 682–737.
(40) Siracusano, S.; Baglio, V.; Di Blasi, A.; Briguglio, N.; Stassi, A.; Ornelas, R.; Trifoni, E.; Antonucci, V.; Arico, A. S. *Int. J. Hydrogen Energy* **2010**, *35* (11), 5558–5568.
(41) Ardizzone, S.; Carugati, A.; Trasatti, S. *J. Electroanal. Chem.* **1981**, *126* (1−3), 287–292.
(42) De Pauli, C. P.; Trasatti, S. *J. Electroanal. Chem.* **2002**, *538*, 145–151.
(43) de Oliveira-Sousa, A.; da Silva, M. A. S.; Machado, S. A. S.; Avaca, L. A.; de Lima-Neto, P. *Electrochim. Acta* **2000**, *45* (27), 4467–4473.
(44) Pauporte, T.; Andolfatto, F.; Durand, R. *Electrochim. Acta* **1999**, *45* (3), 431–439.
(45) Fierro, S.; Ouattara, L.; Calderon, E. H.; Comninellis, C. *Electrochem. Commun.* **2008**, *10* (6), 955–959.
(46) Fierro, S.; Kapalka, A.; Comninellis, C. *Electrochem. Commun.* **2010**, *12* (1), 172–174.